

FlowGNN: A Dataflow Architecture for Universal Graph Neural Network Inference via Multi-Queue Streaming

Rishov Sarkar, Stefan Abi-Karam, Yuqi He, Lakshmi Sathidevi, Cong Hao
 School of Electrical and Computer Engineering, Georgia Institute of Technology
 {rishov.sarkar, stefanabikaram, yhe374, lsathidevi3, callie.hao}@gatech.edu

ABSTRACT

Graph neural networks (GNNs) have recently exploded in popularity thanks to their broad applicability to graph-related problems such as quantum chemistry, drug discovery, and high energy physics. However, meeting demand for novel GNN models and fast inference simultaneously is challenging because of the gap between developing efficient accelerators and the rapid creation of new GNN models. Prior art focuses on the acceleration of specific classes of GNNs, such as Graph Convolutional Network (GCN), but lacks the generality to support a wide range of existing or new GNN models. Meanwhile, most work rely on graph pre-processing to exploit data locality, making them unsuitable for real-time applications. To address these limitations, in this work, we propose a generic dataflow architecture for GNN acceleration, named **FlowGNN**, which can flexibly support the majority of *message-passing* GNNs. The contributions are three-fold. First, we propose a novel and scalable *dataflow* architecture, which flexibly supports a wide range of GNN models with message-passing mechanism. The architecture features a configurable dataflow optimized for simultaneous computation of node embedding, edge embedding, and message passing, which is generally applicable to all models. We also propose a rich library of model-specific components. Second, we deliver ultra-fast real-time GNN inference without *any* graph pre-processing, making it agnostic to dynamically changing graph structures. Third, we verify our architecture on the Xilinx Alveo U50 FPGA board and measure the *on-board end-to-end* performance. We achieve a speed-up of up to $51\text{--}254\times$ against CPU (6226R) and $1.3\text{--}477\times$ against GPU (A6000) (with batch sizes 1 through 1024); we also outperform the SOTA GNN accelerator I-GCN by $1.03\times$ and $1.25\times$ across two datasets. Our implementation code and on-board measurement are publicly available on GitHub.¹

1. INTRODUCTION

Graph Neural Networks (GNNs) have become a powerful tool for applying deep learning to solve tasks infilling graph structures. Learning tasks for graphs can be applied at node-level (e.g., presence of protein [40]), edge-level (e.g., drug-drug interactions [47]), and graph-level (e.g., molecular property prediction [49]). Representative applications of GNNs include analysis of social networks and citation networks, recommendation systems, traffic forecasting, LIDAR point cloud segmentation for autonomous driving, high en-

ergy particle physics, molecular representations, and drug discovery [2].

Targeting various applications, there is a huge demand for GNN inference acceleration with different requirements, where **real-time** processing is an essential one with increasing needs. For instance, point cloud segmentation and detection for autonomous driving using GNNs [38] require real-time computation. Another concrete example is that, in high energy particle physics, the collision data from particle collider are collected every 25ns and thus must be processed using GNNs within nanoseconds with raw input graphs [5, 21, 39]. Consequently, GNN acceleration is critical to these applications with dynamically changing graph inputs to deliver real-time computation, where there is no time for graph pre-processing or graph-specific optimizations.

The **challenges** and the **limitations** of existing accelerators, however, are significant. First, GNN computation is both communication-intensive and computation-intensive, as also noted by previous literature [3, 29, 60]; GNN involves both massive irregular memory access for message passing and heavy computation for embedding transformation, which is the major difference from traditional graph processing frameworks. Second, novel GNN models are rapidly emerging while accelerator innovation is lagging behind. For instance, most state-of-the-art (SOTA) GNN accelerators are tailored for graph convolutional networks (GCNs) [13, 15, 59, 60], which can be conveniently expressed as sparse matrix multiplications (SpMM). However, the majority of GNNs are *not* suitable for SpMM because of complicated operations such as edge embedding, attention, mixed neighborhood aggregation, etc. Therefore, *generic, extensible, and flexible acceleration frameworks* are required to rapidly adapt to evolving GNN models. Third, some accelerators adopt graph preprocessing to enhance data locality [6, 23, 46, 53, 60], while some apply graph partitioning relying on the property of a fixed input graph (e.g., by analyzing the adjacency matrix sparsity [59]). Such preprocessing or graph-specific techniques *are not feasible* for real-time applications with millions of input graphs with varied structures.

Motivated by the emerging requirements and existing limitations, we propose a generic and flexible architecture for GNN acceleration, named **FlowGNN**, which supports a wide range of prevailing GNNs with message-passing mechanism and is easily extensible for new models. Highlighting the three features of FlowGNN in Table 1, we summarize our contributions as follows:

- **Generic.** (1) *Model-generic*. FlowGNN is the first generic GNN accelerator that can process the majority of state-of-the-art GNNs by supporting the *message passing* mecha-

¹<https://github.com/sharc-lab/FlowGNN>

Table 1: Comparisons between our FlowGNN framework and existing GNN accelerators; our main features are: *generic* – supports a wide range of message-passing GNNs; *real-time* – does not require any pre-processing; *open-source* – with on-board measured end-to-end performance with guaranteed functionality.

Feature	SOTA GNN Accelerators	Ours (FlowGNN)
Generic	✗: GCN only [59, 60] ✗: Do not support edge embeddings [14, 15, 30, 54] ✗: Rely on graph-specific property (e.g., sparsity) [59]	✓: Support a wide types of GNNs with message-passing ✓: Support edge embeddings, attention, multi-aggregation, etc. ✓: Agnostic to GNN models, datasets, and graph structures
Real-time	✗: Requires heavy graph preprocessing [60] or partitioning on CPU [59]	✓: Zero preprocessing; directly takes in raw graphs in a streaming fashion and processes on-the-fly
Open-source	✗: Not available yet	✓: Implementation open-sourced with executables

Table 2: Supported representative GNNs by our framework FlowGNN with flexible extensions.

Model	SOTA	Ours	Representativeness
GCN [27]	✓ [15]	✓	GNN family that can be represented as sparse matrix-matrix multiplications (SpMM)
GIN [50] [20]	✗ [15]	✓	GNN family with <i>edge embeddings</i> and transformations where SpMM <i>does not</i> apply
GAT [43] [3]	✗ [3]	✓	Anisotropic GNN family with sophisticated message functions
PNA [9]	✗	✓	A popular GNN family arbitrarily using multiple aggregation methods
DGN [4]	✗	✓	A state-of-the-art GNN with a directional flow at each node and guided aggregation
VN [16]	✗	✓	A widely used GNN technique with a virtual node connecting to all other nodes

GCN: graph convolutional network; **GIN**: graph isomorphism network; **GAT**: graph attention network; **PNA**: principal neighbourhood aggregation; **DGN**: directional graph network; **VN**: GNN with virtual node. ✗: Discussed in SOTA accelerators but is *not* applicable with *edge embeddings*.

nism. Table 2 summarizes the currently supported GNN models, each being representative of a large GNN family. In particular, we emphasize that FlowGNN supports *edge embeddings*, which is not considered by existing accelerators but is widely used in most GNN models. (2) *Graph-generic*. FlowGNN is also dataset and graph structure agnostic; its optimizations do not rely on analysis for a specific input graph, but can consecutively and effectively process a series of graphs with arbitrary structure.

- **Real-time.** FlowGNN targets *real-time* applications with *zero preprocessing* and partitioning, where the graphs are streamed in consecutively and processed on-the-fly.
- **Dataflow architecture.** We propose a novel dataflow architecture, which can effectively overlap the two most time-consuming steps in GNN, node transformation and message passing, and significantly reduce processing units’ idle time. To boost the performance, FlowGNN also exploits multiple levels of parallelism: node, edge, scatter, and apply, via a novel multi-queue-based on-the-fly multicasting adapter.
- **Open-source and modularized.** The implementation of FlowGNN architecture is publicly available, with on-FPGA measurement and guaranteed end-to-end functionality by

cross-checking with PyTorch implementations. It also includes a rich library of model-specific modules, where new GNN components can be developed and plugged into FlowGNN seamlessly.

- **Evaluation.** We verify the proposed architecture on Xilinx Alveo U50 FPGA by measuring its *on-board* performance. We use three popular datasets with more than 43k graphs being streamed into FlowGNN. FlowGNN achieves a speed-up of 54–254× against CPU (6226R) and 1.3–477× against GPU (A6000) with batch sizes from 1024 to 1 with 4× less power. Comparing with the SOTA accelerator I-GCN, we observe 1.03× and 1.25× better performance. The remarkable speedup suggests that *we did not sacrifice performance for generality*, given that the goal of FlowGNN is a general framework for advanced GNNs.

2. RELATED WORK AND MOTIVATIONS

2.1 Related Work

GNN acceleration is attracting intensive attention in the research community. Recent works are summarized by a survey [1], including accelerations using CPU/GPUs, ASICs, FPGAs, and heterogeneous platforms. Auten et al. [3] propose the first GNN accelerator composed of four modules: graph traversal, matrix operation, data scheduling, and graph aggregations. HyGCN [54] is also among the earliest of these using a hybrid architecture for GCN acceleration with dedicated modules for aggregation and combination. AWB-GCN [14] is an FPGA accelerator that aims to combat workload imbalance in graph processing. EnGN [31] uses PEs connected in a ring and performs aggregations using a technique called Ring-Edge Reduce, while GRIP [26] uses the GReTA abstraction [25] to enable acceleration of any GNN variant. GCNAX [28] addresses the shortcomings of resource underutilization and excessive data movement using a flexible dataflow. Rubik [7] and GraphACT [57] aim to accelerate GCN training using ASIC and FPGA, respectively. Boost-GCN [59] specifically optimizes GCN via sparsity analysis and graph partitioning. I-GCN [15] is the most recent GCN accelerator delivering the state-of-the-art performance, which uses an islandization approach to de-duplicate redundant GCN computations by merging nodes with shared neighbors.

Complementary to GNN acceleration, another category of related work is general graph processors, such as GraphH [10], Blogel [52], Giraph++ [42], ForeGraph [11], FabGraph [36], HitGraph [61], AccuGraph [55], and the most recent open-

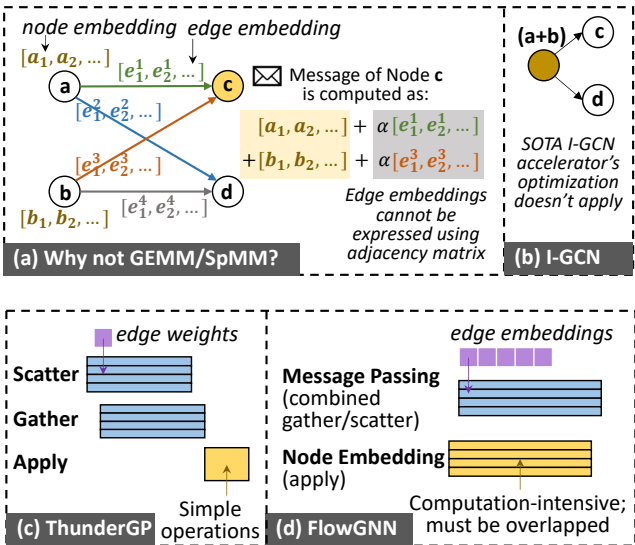


Figure 1: (a) GNNs cannot be expressed as a sequence of GEMM and SpMM if there are edge embeddings. (b) Because of edge embeddings, redundancy removal by node merging in I-GCN [15] is not applicable. (c) SOTA graph processor ThunderGP [8] with pipelined scatter and gather, followed by a graph-level apply. In GNNs, however, the Node Transformation (apply) is usually computation-intensive (e.g., MLP) and thus must be efficiently overlapped. (d) Our FlowGNN achieves this by a novel and scalable dataflow architecture.

source framework ThunderGP [8]. General graph processing usually follows the gather-apply-scatter model, where common applications include PageRank, sparse matrix vector multiplication, breadth-first search, single source shortest path, weakly connected component, etc.

2.2 Limitations

Despite the great success of existing GNN accelerators and general graph processors, there are still limitations being overlooked. The most significant one is that, **advanced GNNs cannot be simplified as matrix multiplications, and edge embeddings cannot be ignored**. The majority of existing GNN accelerators mainly focus on Graph Convolutional Networks (GCNs) and simplify the computation as a series of sparse and general matrix multiplications (SpMM and GEMM), so that most accelerators focus on optimizing SpMM/GEMM kernels. However, this simplification is *not valid* for many reasons, such as edge embedding (a result of edge attributes), complex aggregators, anisotropic GNNs, and heterogeneous GNNs, etc. Moreover, incorporating edge embeddings will invalidate some optimization techniques. More specifically, we list three cases as examples where SpMM/GEMM representation is not applicable:

- **Edge embedding.** Edge embeddings are used to represent important edge attributes, such as chemical bonds in a molecule [17, 56] or relationships in social networks. A simple GCN can be computed using a series of GEMM

using a graph’s adjacency matrix, if there are no edge attributes or only has scalar edge weights. However, if there are multi-dimensional edge features, the SpMM/GEMM formulation no longer holds. For example, GIN [20] with edge embeddings is formulated as below:

$$x_i^{l+1} = \text{MLP}((1 + \varepsilon) \cdot x_i^l + \sum_{j \in \mathcal{N}(i)} \text{ReLU}(x_j^l + e_{j,i}^l))$$

where $x_i \in \mathbf{X}$ is node embedding and $e_{j,i} \in E$ is edge embedding. Because the feature matrix $X^{N \times F}$ and edge embedding matrix $E^{M \times D}$ are of different sizes (F, D : embedding dimensions; N : number of nodes; M : number of edges), the values have to be added differently. Fig. 1(a) demonstrates the computation with edge embeddings.

Additionally, the existence of edge embeddings prevent some GNN optimization techniques from being applicable. For example, the SOTA GCN accelerator, I-GCN [15], proposes a redundancy removal approach by merging nodes with same neighbors to reduce computation, as shown in Fig. 1(b) by merging node a and b . However, with edge embeddings, the messages from a to c and from b to c are no longer the same as those from a to d and b to d , and thus a and b cannot be merged.

- **Non-trivial aggregation.** GNNs using aggregations besides summation are inexpressible as SpMM. For instance, the Principal Neighborhood Aggregation (PNA) GNN in our framework uses mean, standard deviation, min, and max aggregations altogether in a weighted manner; it cannot be written as GEMM or SpMM since it is no longer “summation” after multiplication. More formally, to be expressed as standard matrix multiplication, the formulation needs to be in the format of semi-ring $(\times, +)$ [24]. With non-sum aggregation, for example max aggregation, the semi-ring will be defined as (\times, \max) and thus GEMM/SpMM do not apply.

- **Anisotropic GNNs.** Anisotropic GNNs require that a neighboring node transformation shall depend on the neighboring node and target node [41]. While for isotropic GNNs, propagation can be implemented using matrix multiplication-style approaches, for anisotropic ones, messages must be explicitly materialized [41]. One example is Graph Attention Networks (GAT) in our framework. In a GAT layer, a neighboring node is scaled by an attention coefficient α , which is dynamically computed depending on all other neighboring nodes. This dynamic nature prevents the GAT from being expressed as matrix multiplications.

Therefore, existing accelerators, which heavily focus on GCN, rely on SpMM/GEMM formulation, and ignore edge embeddings, can greatly limit their generalization to advanced and emerging new GNNs, such as GAT, GIN, PNA, etc., as listed in Table 2. In addition, many existing accelerators apply graph *pre-processing* to exploit data locality or partitioning on CPU, such as GraphACT [58], HyGCN [54], VersaGNN [37], and BoostGCN [59]. Such pre-processing are usually excluded from performance measurement and can be impractical for real-time applications where different graphs are consecutively streamed in.

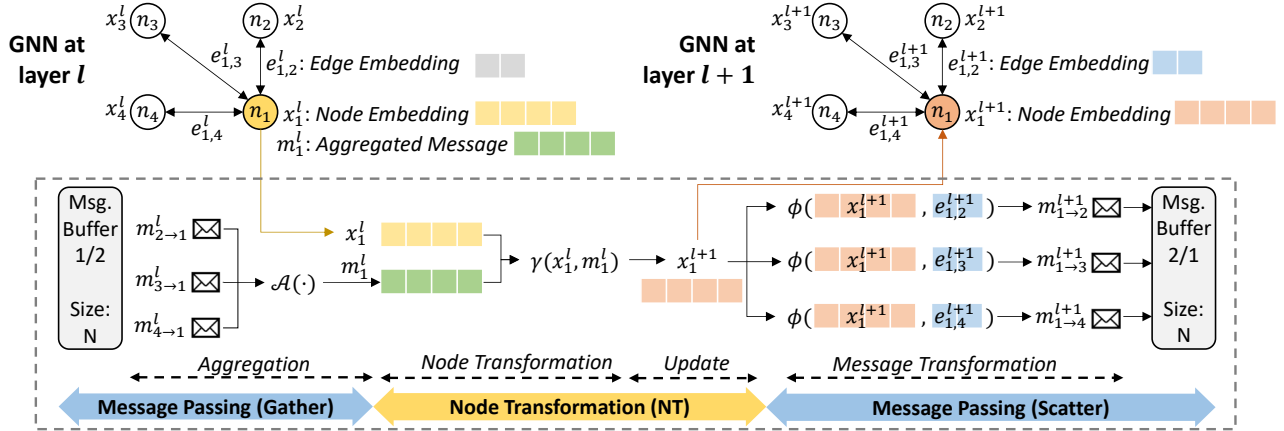


Figure 2: The generic message passing mechanism of prevailing GNN models. It has two major stages: Node Transformation (NT) and Message Passing (MP). NT is analogous to apply and MP is analogous to scatter/gather. Both NT and MP are usually computation-intensive, especially NT, which typically uses linear or multi-layer perceptron (MLP).

2.3 Motivations and Innovations

Motivated by the above limitations, our goal is to develop a *generic and flexible architecture* that can support a wide range of GNNs and can rapidly adapt to emerging GNNs in the future. The main feature of our proposed framework is an **explicit message passing mechanism** that significantly improves the generality of the GNN accelerator for several reasons. First, the advantage of message passing is that, it allows one to express almost all GNN architectures at the theoretical formulation level, as pointed out by a recent work [44], that “any function of interest we want to compute over graphs can, in all likelihood, be expressed using pairwise message passing.” Second, explicit message passing allows easy integration of edge embeddings and different aggregation functions into the framework, without changing the fundamental architecture. We demonstrate the great generality of FlowGNN using six different GNN models (Table 2).

Efficiently supporting message passing is non-trivial, however, given the nature of irregular memory access pointed out by a lot of existing literature, since we can no longer exploit the mature SpMM/GEMM optimization techniques. The requirement of *real-time* elevates the challenge since we cannot apply any pre-processing to enforce data locality (except for light-weight on-chip pre-processing).

Given these challenges, our key innovation for high performance is a novel **multi-queue-based dataflow architecture**, which can effectively pipeline the processing of node transformation and edge embedding, the two most computation-intensive steps in GNN, with multiple levels of parallelism. In the experiments, all the performance boost comes from our architectural innovation without any pre-processing or graph manipulation tricks. Nevertheless, our proposed architecture is orthogonal to certain optimization techniques such as on-the-fly partitioning and can be applied together.

Since we explicitly support message passing, which is similar to the gather-apply-scatter (GAS) model in general graph processing, a natural question is how FlowGNN is different from GAS processors. Fig. 1(c) and (d) demonstrate the major difference between the SOTA graph processor ThunderGP [8] and our proposed FlowGNN. In Thun-

derGP, the major performance improvement comes from the pipelined scatter and gather, followed by apply. This is acceptable because in graph processing, apply usually is a simple operation such as scalar summation. In GNN, however, both message passing (analogous to gather/scatter) and node transformation (analogous to apply) are computation intensive, and thus must be effectively pipelined, as we emphasize in FlowGNN.

3. GENERIC ARCHITECTURE

In this section, we introduce the generic dataflow architecture of FlowGNN, including background of message passing mechanism of GNNs (Sec. 3.2), a baseline architecture using simple dataflow without node/edge level parallelism (Sec. 3.3), and an improved FlowGNN with multiple levels of parallelism via data queues (Sec. 3.4). In the next section, we introduce model-specific components for various GNNs.

3.1 FlowGNN Framework Features

FlowGNN Features. Our goal is to provide a generic and real-time GNN acceleration architecture with great flexibility to support a wide range and emerging GNNs with minimum modifications. Table 1 summarizes our key features compared with state-of-the-art accelerators. **① Generic.** While most existing accelerators are limited to GCN by formulating GNN computation as SpMM, FlowGNN supports a wide variety of GNN types by constructing a *message passing* architecture to which most GNNs belong. It can also accept arbitrary dataset and graph structures. **② Real-time.** In practical applications such as point clouds in autonomous driving and particle graphs in high energy physics, the graphs are constructed and must be processed in real-time, leaving no time for pre-processing, partitioning, or adjacency matrix analysis. Different from accelerators that rely on a preprocessing/partitioning optimization, FlowGNN directly processes raw graphs consecutively, targeting real-time inference for a large number of graphs. **③ Open-source.** We open-source the FlowGNN implementation to encourage more GNNs to be built on top of it to promote a GNN acceleration ecosystem.

Notation	Description
$\mathcal{G} = (A, X, E)$	The input graph for the GNN
$A \in \mathbb{R}^{N \times N}$	Adjacency matrix of \mathcal{G} (N : number of nodes)
$x_i^l \in X \in \mathbb{R}^{N \times F}$	Node embedding of node i at layer l
$e_{i,j}^l \in E \in \mathbb{R}^{M \times D}$	Edge embedding of edge i, j at layer l
F, D	Dimension of node and edge embeddings
$\mathcal{N}(i)$	All neighbors of node i
$\phi(\cdot)$	Differentiable message transformation function
$\mathcal{A}(\cdot)$	Permutation-invariant aggregation function
$\gamma(\cdot)$	Differentiable node transformation function

Table 3: Notations used in GNN definition.

Supported GNNs. Table 2 summarizes currently supported GNNs, each being representative of a family of GNNs. Graph convolutional network (GCN) [27] represents those which can be formulated as sparse matrix-matrix multiplications (SpMM); simplified GCN [48] also falls into this category. Graph isomorphism network (GIN) [50] represents advanced GNNs with higher representation power, *including edge embeddings* and transformations where SpMM *does not apply*; GraphSage [18] falls into this category. Principal neighborhood aggregation (PNA) [19] represents a popular GNN family that uses multiple arbitrary aggregation methods simultaneously. Graph attention network (GAT) [43] represents the anisotropic GNN family with sophisticated message functions, in which edges must be materialized [41]. Directional graph network (DGN) [4] is a state-of-the-art GNN with directional flow at nodes with guided aggregation. GNN with virtual node (VN) [16] is a widely used GNN technique using virtual nodes connected to all other nodes.

3.2 Message Passing Mechanism

Most prevailing GNN architectures follow the message passing mechanism [4, 9, 12, 16, 18, 27, 43, 45, 48, 50]. With notations defined as in Table 3, the general computation of a message passing GNN can be expressed as:

$$x_i^{l+1} = \gamma(x_i^l, \mathcal{A}(\phi(x_i^l, x_j^l, e_{i,j}^l)))$$

Fig. 2 demonstrates the message passing procedure for a single node n_1 at layer l , which will be repeatedly applied for all nodes and for several layers. Highlighted at the bottom of the figure, there are two major steps for each node in each layer of the GNN: **message passing (MP)** and **node transformation (NT)**. Message passing can be divided into gather and scatter phases, where gather corresponds to feature aggregation, and scatter corresponds to message transformation and passing. *Edge embeddings* are incorporated into the message during scatter phase. Node transformation usually uses linear or multi-layer perceptron (MLP), followed by node update.

More specifically, the GNN computation flow has the following stages, as demonstrated in Fig. 2:

Message Passing (Gather). In the gather phase, a.k.a., aggregation, of a certain node n_1 , the messages from its neighboring nodes obtained in the previous layer are retrieved from a message buffer. The messages are then aggregated in a permutation invariant manner, denoted by $\mathcal{A}(\cdot)$ (e.g., sum, max, mean, std. dev.). In advanced GNNs such as

PNA, multiple aggregators are used with learnable weights and scaled according to the degree of the target node. The aggregated message is denoted by m_1^l .

Node Transformation. After aggregation, m_1^l is processed together with node n_1 's current node embedding, denoted by x_1^l , via a node transformation function, $\gamma(\cdot)$. $\gamma(\cdot)$ applies a node transformation using m_1^l and x_1^l , such as identity function, fully-connected layer, weighted sum of m_1^l and x_1^l , or an MLP. After the transformation, $\gamma(\cdot)$ produces a new node embedding of n_1 , denoted by x_1^{l+1} , and applies the update.

Message Passing (Scatter). After node transformation, it is the scatter phase of message passing. The new node embedding x_1^{l+1} will be transformed by a message transformation function, $\phi(\cdot)$, usually together with an edge embedding $e_{src,dest}^{l+1}$, to generate the node's outgoing message. The message will be dispatched to all its neighbors, which will eventually be collected by the gather stage of the next layer.

A complete GNN model may consist of multiple layers, each with message passing and node transformation steps. For graph-level tasks, a global pooling layer is needed, possibly followed by MLP layers for final prediction.

3.3 Baseline Dataflow Architecture

To explicitly support the message passing mechanism, we first propose the baseline dataflow architecture, as shown in Fig. 3(a). It has two major processing components, one Node Transformation (NT) unit (yellow block), and one Message Passing (MP) unit (blue block), where the edge embeddings are computed during MP. There is a node queue, implemented as a FIFO (first-in first-out), between NT and MP; the queue holds nodes (their embeddings) that are after transformation and are ready for message passing. The node queue is the key to enable pipelined NT and MP: as long as the queue is not empty or full, NT and MP can be executed in parallel. We keep the high-level abstraction for NT and MP units for now and will introduce more details in Sec. 3.4.2.

Data Buffers. The architecture has three data buffers: one node embedding buffer and two message buffers, all with N entries. The two message buffers act alternately across layers: during layer 1, message buffer 1 is read-only while message buffer 2 is being updated; during layer 2, message buffer 2 becomes read-only and buffer 1 updates, and so on.

Execution Flow. Fig. 3(a) illustrates the execution flow of one GNN layer; for multiple layers, the same resources and dataflow will be reused. Within one layer, the NT unit takes in one node, e.g., n_1 , together with its received message, applies node transformation and update, e.g., MLP, activation, and self-attention. This is the main component that distinguishes different GNN models. Then, the MP unit performs the subsequent scatter operation for n_1 , by sending out the messages to all n_1 's neighboring nodes. Consider the graph in Fig. 2 as an example. Once node n_1 's embedding is updated, the MP unit retrieves all its neighbors, i.e., n_2 , n_3 , and n_4 , computes the messages together with edge embeddings $e_{1,2}$, $e_{1,3}$, and $e_{1,4}$, and dispatches the messages. The receivers will instantly update their partially aggregated message in the message buffer. In this way, the scatter and gather phases can be merged, because the aggregation function is permutation

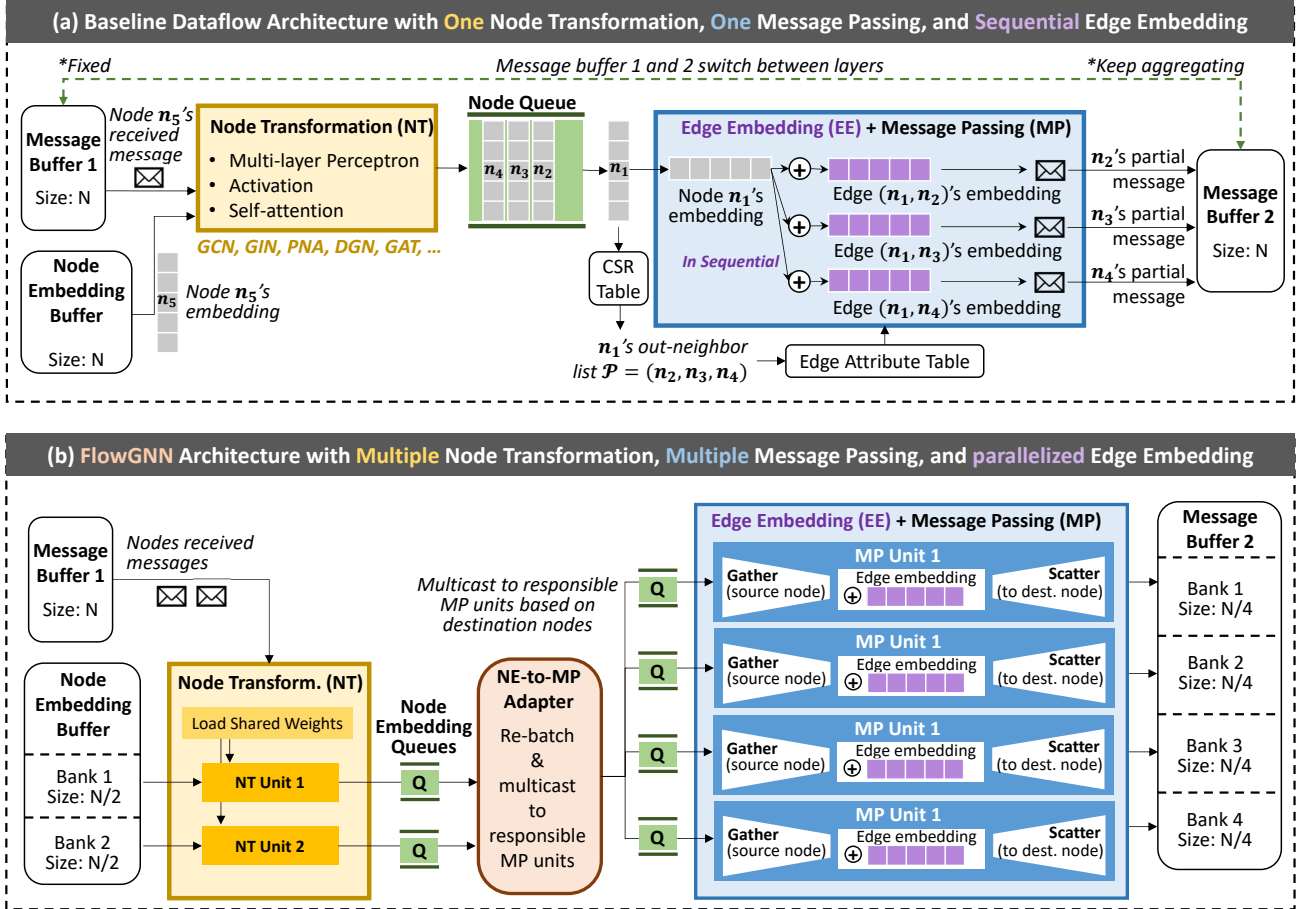


Figure 3: Our proposed baseline dataflow architecture and the improved FlowGNN architecture. (a) The baseline dataflow architecture can effectively pipeline the Node Transformation (NT) and Message Passing (MP), but processes only one node and one edge at a time. (b) The improved FlowGNN architecture can process multiple nodes and multiple edges simultaneously, enabled by an NT-to-MP adapter via on-the-fly multicasting.

invariant and the order of aggregation does not matter. Such a merged fashion has two merits. First, it reduces the overall process latency by fusing two stages into one. Second, it reduces memory cost from $O(E)$ to $O(N)$ where E is the number of edges and is typically much larger than N . This approach requires that the graph data is stored in its compressed sparse row (CSR) format.

Note that an equivalent procedure is to first perform gather, i.e., aggregation, via incoming edges and then perform node transformation, in which case no scatter is needed. This approach requires two node embedding and one message buffer, all of size $O(N)$, and graph data stored in compressed sparse column (CSC) format.

Fig. 4 illustrates different strategies for NT and MP processing. ① **Non-pipeline**. In Fig. 4(a), NT and MP are not pipelined, which apparently suffers from a huge waste of idle cycles. ② **Fixed pipeline**. In Fig. 4(b), NT and MP are pipelined in a fixed manner: NT for the second node is pipelined with MP for the first node, etc. This achieves some latency reduction but suffers from imbalanced NT and MP processing time. Specifically, if some nodes have larger degrees with longer MP latency than NT while others have shorter MP, there still will be idle cycles. ③ **Baseline**

dataflow pipeline. In Fig. 4(c), NT and MP are pipelined flexibly using a node queue: as soon as a node finishes its NT, i.e., is ready for message passing, its embeddings are pushed into the queue; meanwhile, the MP unit reads from the queue, incorporates edge embeddings, and then does scatter. This approach can greatly reduce idle cycles.

Limitations of Baseline Dataflow Architecture. Although the baseline dataflow architecture can effectively pipeline the NT and MP, there are multiple limitations. The most obvious one is that it can process only one node and one edge at a time, while it is highly expected to process multiple nodes and edges simultaneously. The second limitation is that, as shown in Fig. 4(c), NT and MP are not pipelined within one node, meaning that the node cannot start its MP until its NT completes.

3.4 Proposed FlowGNN Architecture

Inheriting the advantages of the baseline dataflow architecture, we propose our FlowGNN architecture to address the limitations and to greatly boost the performance by enabling multiple levels of parallelism. On top of the baseline dataflow architecture, FlowGNN allows the following configurable

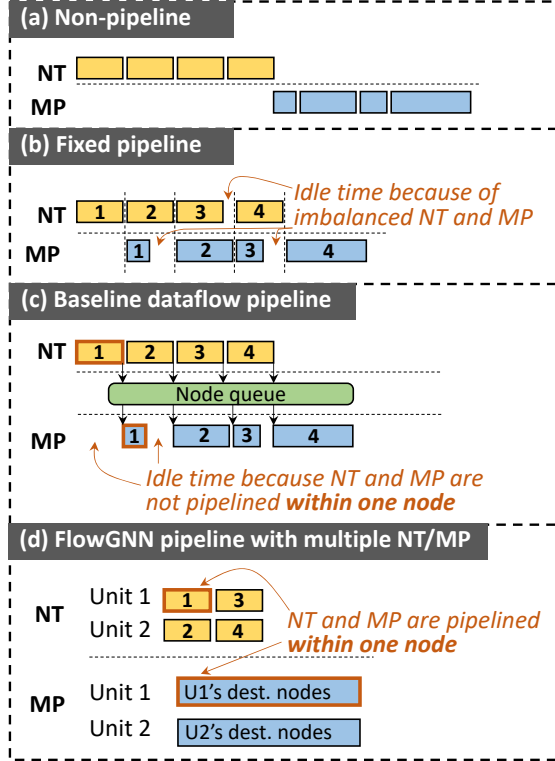


Figure 4: Different strategies of pipelining of node transformation (NT) and message passing (MP). The proposed FlowGNN pipeline in (d) explores node/edge levels parallelism and can pipeline NT and MP within one node.

parallelization parameters:

- Node parallelism, denoted by P_{node} , indicating how many nodes can be processed simultaneously by NT.
- Edge parallelism, denoted by P_{edge} , indicating how many edges can be processed simultaneously by MP.
- Apply parallelism, denoted by P_{apply} , indicating how many node embedding dimensions can be processed simultaneously by one NT.
- Scatter parallelism, denoted by $P_{scatter}$, indicating how many edge embedding dimensions can be processed simultaneously by one MP.

Fig. 3(b) depicts FlowGNN architecture. It has multiple NT units and multiple MP units (2 and 4 in this example; can be configured); between NT and MP is an NT-to-MP adapter, connecting NT units and MP units using multiple data queues. To allow parallel access, the node embedding and message buffers are partitioned into multiple banks. We introduce each component in detail in the following.

3.4.1 Node/Edge Parallelism

The key innovation of FlowGNN over baseline is node and edge parallelism, which is, however, non-trivial. While parallelizing NT across multiple nodes is straightforward, it is challenging to parallelizing MP across multiple edges, because of the random access of reading the edge attributes and writing to the target node embeddings. Specifically, to process message passing for a group of edges in parallel,

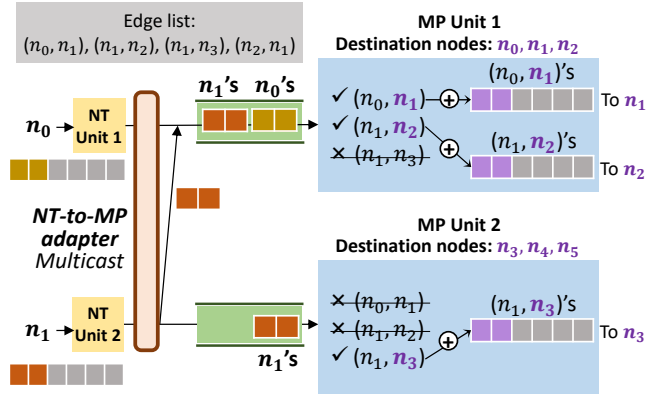


Figure 5: MP units process edges and pass messages based on destination nodes. The NT-to-MP adapter multicasts the node embeddings to the correct MP unit. Note that the MP doesn't wait for the entire node embedding; it starts as soon as the first few elements arrive.

those edges as well as their target nodes must be in different memory banks or buffers; without graph pre-processing, such accesses are random and thus cannot be parallelized.

To address this problem, we propose a novel multi-queue dataflow to enable parallelized NT and MP via on-the-fly node distribution. The key idea is to instantiate multiple NT and MP units, let each MP unit process one particular bank of edges, and write to one particular bank of node embeddings. In this way, multiple NT and MP units can operate in parallel without conflicting.

To achieve this, we design an **NT-to-MP adapter** and perform *on-the-fly multicasting*. Given P_{node} NT units, P_{node} nodes are processed in parallel as one batch. During this batch of NT, the NT-to-MP adapter distributes each node's finished embeddings to its dedicated MP unit to perform the subsequent scatter operations. The multicasting is based on the *target node's ID*, and the edge attributes and node embeddings are also stored in different memory banks based on the target node's ID; in this way, each MP is guaranteed to process a subset of edges and scatter to a subset of nodes within its own bank. This addresses the first limitation of the baseline dataflow architecture. It is worth noting that, for a particular node, MP does not need to wait for its node transformation to complete for all dimensions; as soon as the first few embedding values are computed, those values are streamed into the data queue, from which the MP can start to fetch. This addresses the second limitation of the baseline architecture.

Fig. 5 presents an example of multiple NT and MP units working in parallel via broadcasting. Assume the edge list is $(n_0, n_1), (n_1, n_2), (n_1, n_3)$, and (n_2, n_1) . Given two NT units, n_0 and n_1 are processed in parallel. As soon as their first P_{apply} embedding elements are computed (2 in this example), the NT-to-MP adapter will send them to the data queue which belongs to the correct MP unit. In this example, assume MP unit 1 is responsible for edges whose destination nodes are n_0, n_1 , and n_2 ; MP unit 2 is responsible for edges whose destination nodes are n_3, n_4 , and n_5 . Therefore, since n_0 's neighbor is n_1 , its embeddings should be sent to MP unit 1 only; since n_1 's neighbors are n_2 and n_3 , its embeddings

should be sent to both MP unit 1 and 2. Then, within each MP unit, it only processes its own edges in its own memory bank. When the entire embedding is finished, MP unit 1 scatters to node n_1 and n_2 , while MP unit 2 scatters to node n_3 .

Fig. 4(d) illustrates the ④ **FlowGNN pipeline**. It shows significant improvement over ③, including multiple NT and MP units executing in parallel, and pipelined NT and MP within one node.

3.4.2 Apply/Scatter Parallelism

Node Transformation (NT) Unit. The NT unit handles any per-node computations required for GNN. In most GNN algorithms, this consists of one or more fully-connected layers and activation functions using learnable weights and biases to transform each node’s embedding for each GNN layer.

The canonical implementation of the FlowGNN NT unit consists of two sequential processes, overlapped between nodes using ping-pong buffers to hide latency: accumulate and output. The accumulate process reads each node’s message vector and computes a linear layer in an input-stationary fashion: each fetched element in the message vector is used to update the entire output embedding vector. Then, once the accumulate process has completed for an entire node, the output process can perform any finalization steps, such as an activation function, and write the resulting embedding to both the message buffer and an intermediate FIFO queue to be used for the message passing process.

The NT unit employs embedding-level parallelism using a configurable parameter P_{apply} , which canonically controls the degree of parallelism across the node embedding dimension. This parameter determines the number of elements read from each node’s message vector each cycle and multiplied to produce output node embeddings.

Message Passing (MP) Unit. The MP units handle per-edge computations for each GNN algorithm. Two configurations of an MP unit are supported, depending on whether a particular GNN model is more suited to an NT-to-MP (i.e., transform, then scatter) dataflow or an MP-to-NT (i.e., gather, then transform) dataflow.

In the NT-to-MP dataflow, each MP unit handles an independent subset of *destination* nodes, as discussed in Sec. 3.4.1; analogously, in the MP-to-NT dataflow, each MP unit is assigned a subset of *source* nodes, gathering partial messages along edges from nodes within the assigned subset.

The MP unit also employs a configurable parameter P_{scatter} , determining the degree of parallelism across the edge embedding dimension. Notably, if P_{apply} and P_{scatter} are not the same, the NT-to-MP adapter will re-batch the embedding elements for alignment. For example, if $P_{\text{apply}} = 1$ and $P_{\text{scatter}} = 4$, the adapter will collect 4 elements from NT and then send to MP.

4. MODEL-SPECIFIC COMPONENTS

In this section, we introduce model-specific optimizations on top of the general message passing architecture.

Graph Isomorphism Network. GIN is representative of the GNN family whose message passing involves edge embeddings, and whose node transformation is computation intensive using MLPs. Each node’s outgoing message is a

weighted sum of its own node embedding and the outgoing edge embedding. Its message passing is within the framework using a customized message transformation function $\phi(x, m) = x^l + \epsilon^l \cdot m^l$.

GIN can take special advantage of the two-process NT implementation to compute its two-layer MLP node transformation without incurring any additional latency. The two layers are computed consecutively during the two processes described in Sec. 3.4.2; the second layer is computed in an output-stationary manner.

Graph Attention Network. GAT is representative of anisotropic GNNs because of its multi-head self-attention: each node’s incoming messages are first weighted before aggregation, where the attention coefficients are computed using the node and its neighbor’s embeddings. This exposes additional computation complexity, but fortunately, GAT is still fully compatible with FlowGNN. Similar to GIN, GAT also needs a customized message transformation function, where $\phi(x, m) = x_i^l + \sigma_{i,j}^l \cdot m_j^l$, where $\sigma_{i,j}$ is the attention coefficient from node j to node i , computed using an attention function $\sigma_{i,j} = A(x_i, x_j)$ such as weighted sum or MLP.

Principled Neighbor Aggregation. PNA uses multiple neighbor aggregations to increase the distinguishing power, where the node embedding is computed as follows: [9]:

$$x_i^{l+1} = \text{ReLU}(\text{linear}(\bigoplus_{j \in \mathcal{N}(i)} (x_j^l)))$$

$$\bigoplus = \begin{bmatrix} 1 \\ \log(D_i + 1)/\tilde{D} \\ \tilde{D}/\log(D_i + 1) \end{bmatrix} \otimes \begin{bmatrix} \mu \\ \sigma \\ \max \\ \min \end{bmatrix}$$

where D_i is the degree of x_i and \tilde{D} is the average node degree seen in training data.

PNA falls into the message passing framework with a difference at the aggregation function. It has four aggregators including min, max, mean, and standard deviation; each aggregator stores its results into a separate buffer. All the scaling values are then computed and multiplied with the four aggregation values and written into a global buffer. Lastly, a pipelined linear-ReLU kernel is applied to compute the new node embedding, which reuses the MLP in the GIN model. Skip connections are added after each PNA layer computation to copy and accumulate embeddings from the output of the previous layer.

Directional Graph Networks. DGN [4] uses vector fields in a graph to define directional flows at each node that can be used for graph convolutions using anisotropic kernels. It uses eigenvectors of the graph Laplacian matrix to define directional aggregation matrices used in message passing.

Similar to its PyTorch implementation, DGN accepts the precomputed Laplacian eigenvectors as parameters and uses them to compute the relevant directional aggregation matrices on-the-fly during message passing. DGN uses two aggregations: the mean, and the directional derivative aggregation along the first eigenvector as $Y^l = \text{concat}\{D^{-1}AX^l, |B_{dx}^l X^l|\}$ where Y^l is the aggregated messages, the $X^{(l)}$ is the node embeddings, D is the degree matrix, A is the adjacency matrix, and B_{dx}^l is the directional derivative matrix along first eigenvector. FlowGNN is trivially extensible to other types of DGN aggregations, including directional smoothing B_{av} .

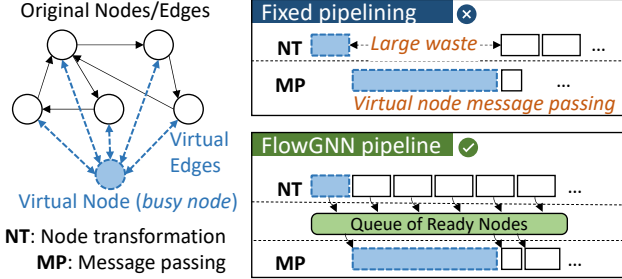


Figure 6: FlowGNN’s dataflow architecture is especially beneficial for models with virtual nodes.

Model	DSP	LUT	FF	BRAM
Available	5,952	872K	1,743K	1344
GIN	1,741	262,863	166,098	204
GCN	1,048	229,521	192,328	185
PNA	2,499	205,641	203,125	767
GAT	2,488	148,750	134,439	335
DGN	1,563	200,602	156,681	462

Table 4: Resource utilization on Xilinx Alveo U50 FPGA. The clock frequency is 300 MHz.

DGN’s node transformation uses an MLP with skip connections similar to PNA.

Virtual Node. Our dataflow architecture for pipelined node and edge processing is especially beneficial for models with virtual nodes. A virtual node [16] is an artificial node connected to all other nodes in the graph. It provides a shortcut for message passing between node pairs, which is demonstrated to be effective in many GNN models [22, 33, 51]. As illustrated in Fig. 6 left, a virtual node is *busy* with connections to all nodes, which results in highly unbalanced workloads especially for large graphs and thus requires special processing. In some models, there can be multiple virtual nodes [51] which escalates the model complexity.

Fortunately, benefiting from the proposed dataflow pipelining, the imbalance introduced by virtual nodes can be easily resolved without changing the framework. As shown in Fig. 6 right top, in fixed-pipeline or no-pipeline architectures, the process for the virtual node itself will take much longer time than others, resulting in a large waste. In contrast, as shown in Fig. 6 right bottom, in the dataflow architecture, processing of the virtual node can be fully overlapped with the node embedding computation for other nodes, with zero waste, as long as it is processed early enough (depending on the node ID numbering and processing order, which is adjustable).

5. EXPERIMENTS

5.1 Model and Implementation Details

We implement our FlowGNN for all six models on Xilinx FPGA Alveo U50 accelerator card using High-Level Synthesis (HLS) by Vitis HLS and Vivado. The available resources of U50 is shown in Table 4, and the FPGA logic targets 300 MHz clock frequency. The graphs are streamed into the accelerator in their raw edge-list format (i.e., COO) consecutively with zero CPU intervention.

As listed in Table 2, we implement six GNN models, each being representative to a family of GNNs. Notably, each GNN model has a PyTorch version of implementation, to which we cross-check our on-board implementation and guarantee that our end-to-end execution is correct. For GCN, GIN, and GIN+VN, the number of layers is 5 and the node embedding dimension is 100, as specified in the PyTorch model [32]. All of these models also use global average pooling, and an output head with a single linear layer. For PNA, we use 4 layers with an node embedding dimension of 80, global average pooling, and an MLP-ReLU head with sizes (40, 20, 1). For DGN, we use 4 layers and a node embedding dimension of 100, global average pooling, and an MLP-ReLU head with sizes (50, 25, 1). For GAT, we use 5 layers with 4 heads and 16 features per layer, global average pooling, and an output head with a single linear layer. The resource utilization of all models are reported in Table 4.

The latency is measured *end-to-end on-board*, obtained from the “average execution time” in the OpenCL summary report after the execution of all testing graphs.

5.2 Dataset and Baseline

Datasets. We use three datasets to evaluate FlowGNN. For real-time processing evaluation, we adopt two molecular property prediction datasets, MolHIV and MolPCBA, from the Open Graph Benchmark [19]. MolHIV testing set has 4k graphs and MolPCBA testing set has 43k graphs. We also evaluate on two prevailing benchmarks for GNN acceleration, CiteSeer and Cora [35].

Baselines. We take CPU (Intel Xeon Gold 6226R) and GPU (NVIDIA RTX A6000) executions as the baseline. We average five iterations of the time measured on CPU and GPU, where each model is implemented in PyTorch Geometric [34] with identical hyperparameters to their corresponding accelerator with batch size from 1 up to 1024. We also compare with the state-of-the-art accelerator, I-GCN [15], following their experiment settings. Worth noting, as discussed in Sec. 2.2, I-GCN employs a redundancy removal technique that skips explicit materialization of groups of edges, which cannot be used when there are edge embeddings; therefore, this is *not a fair comparison* since I-GCN will fail in many cases where FlowGNN can manage. Nevertheless, we still make effort to make a comparison. For other GNN accelerators such as [59, 60], we find it hard to figure the GNN details such as the number of layers, node embedding dimensions, and whether graph/weight loading and graph-level processing are included. More importantly, our focus is a new framework that can generalize to a wide range of GNN models and can handle more complicated edge embeddings and aggregations, which are neglected in existing works. Therefore, our main comparison is with CPU and GPU using on-board measured performance with functionality guarantee.

5.3 End-to-end Evaluation

We fully evaluate FlowGNN using six GNN models by comparing with CPU and GPU baselines. The latency of FlowGNN is measured **on-board end-to-end**, including weight loading and every graph loading. The reported latency is av-

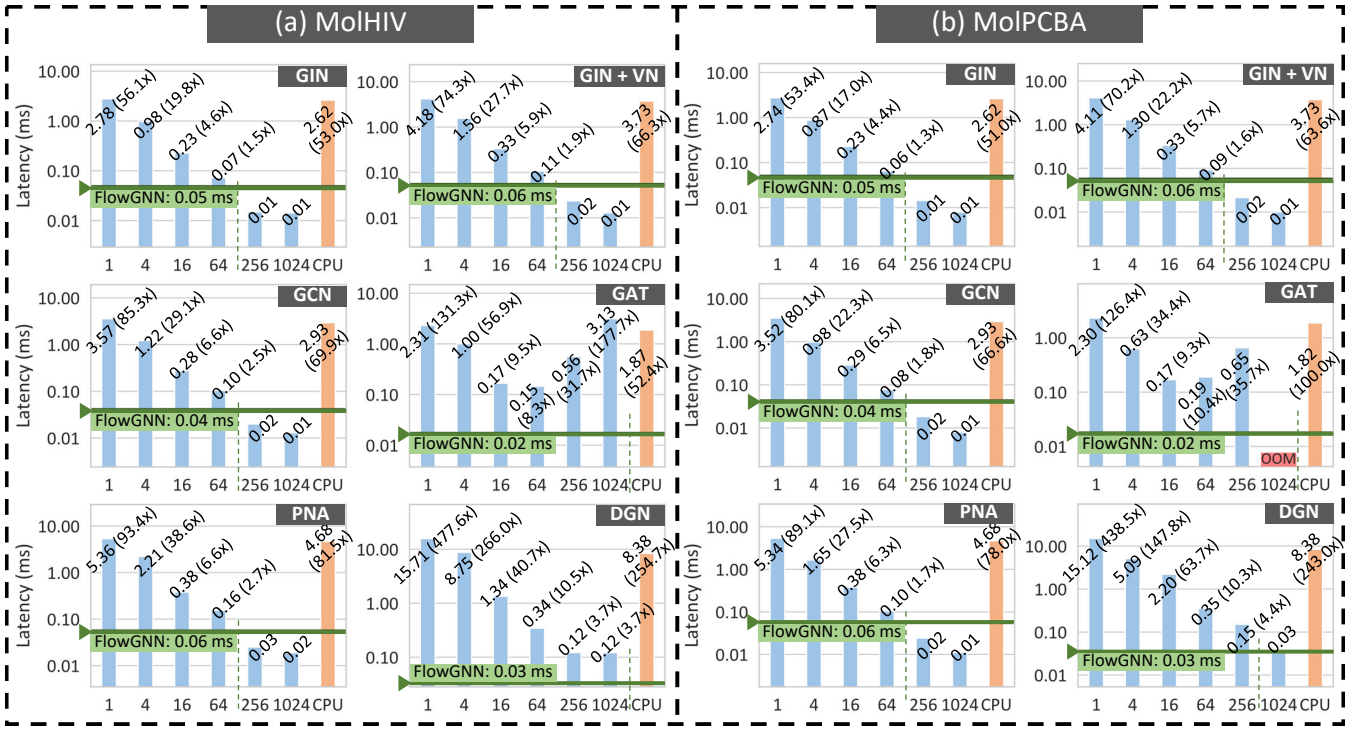


Figure 7: FlowGNN latency measured on-board averaged from 40k test graphs. X-axis is GPU/CPU batch size; Y-axis is the average latency (ms) per graph. GPU baseline is evaluated with batch sizes from 1 to 1024. CPU is evaluated at batch size 1. (a) MolHIV results. (b) MolPCBA results. Our FlowGNN outperforms GPU by 3.58–477× and is consistently faster than GPU with batch size ≤ 64 ; the GAT and DGN models even outperform GPU under batch size 1024.

eraged from all test graphs.

The results are depicted in Fig. 7. The left figure uses the MolHIV dataset, with 4k test graphs, and the right figure uses the MolPCBA dataset, which has 40k test graphs. In each figure, x-axis is GPU/CPU batch size; y-axis is the average latency per graph in milliseconds. GPU baseline is evaluated with batch sizes from 1 to 1024, and CPU is evaluated at batch size 1.

It clearly shows that, for six GNN models, on both datasets, FlowGNN achieves remarkable speedup comparing with CPU and GPU. Comparing with CPU, FlowGNN is 51.0–254.7× faster. Comparing with GPU, FlowGNN is 53.4–477.6× faster at batch size 1. Additionally, FlowGNN is consistently faster than GPU with batch size less or equal to 64, from 1.3× to 266.0×. The GAT and DGN models even outperform GPU under batch size 256 and 1024: GAT being 31.7–177.7× faster, and DGN being 3.7–4.4× faster.

We also evaluated the performance of FlowGNN using five GNN models (no virtual node) on two popular benchmarks for GNNs, Cora and CiteSeer. Results are shown in Fig. 8. It shows that on both graphs, FlowGNN consistently outperforms CPU and GPU (batch size 1 since there is only one graph). In particular, the GAT and DGN models achieve massive speedups of 37.8× and 127.4× respectively over their GPU baselines on Cora and 69.6× and 98.7× over their GPU baselines on CiteSeer.

The remarkable speedup demonstrates the effectiveness of our proposed dataflow architecture, especially without any

pre-processing. In addition, although the goal of FlowGNN is a generic framework, the superior results suggest that *we did not sacrifice performance for generality*.

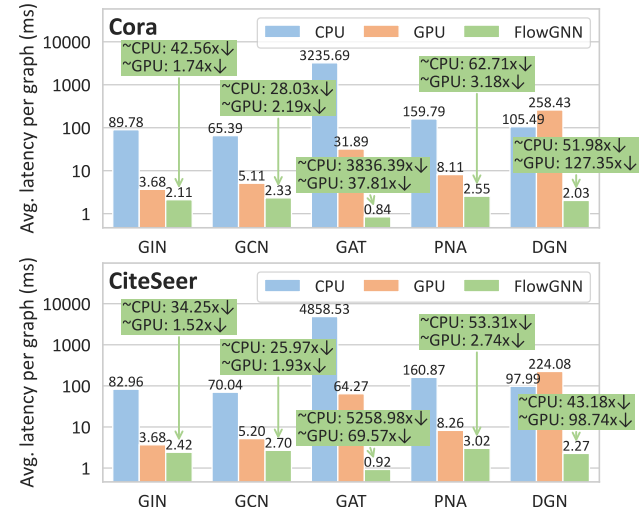


Figure 8: FlowGNN latency on the Cora and CiteSeer datasets, compared against CPU and GPU baselines.

5.4 Ablation Study

We conduct an ablation study to quantitatively evaluate

the proposed techniques of the baseline dataflow architecture as well as the FlowGNN architecture. This experiment uses GCN model on MolHIV dataset. Fig. 9 demonstrates the incremental improvements over the most naive framework, non-pipelined NT and MP (Fig. 4(a), Sec. 3.3). The yellow bars are speedup values against GPU with batch size 1; the blue bars are speedup values against non-pipelined NT and MP. It shows that because of our customized NT and MP units with default parallelism (e.g., parallelized linear and MLP), the non-pipelined NT and MP scheme has already achieved $4.91 \times$ faster than the GPU. Next, it shows that fixed-pipeline is $1.66 \times$ faster than the non-pipeline scheme, while the Baseline Dataflow is another $1.38 \times$ faster because of reduced idle cycles of NT and MP. Then, the FlowGNN-1-1 ($P_{\text{apply}} = 1$, $P_{\text{scatter}} = 1$) is $1.45 \times$ faster than the Baseline Dataflow, because of the pipelined NT and MP for one node, i.e., the MP of one node does not need to wait till its entire NT is finished. We further increase the P_{scatter} from 1 to 2 and P_{apply} from 1 to 2, leading to $1.48 \times$ and $1.02 \times$ improvement, respectively. This ablation study demonstrates that our proposed baseline dataflow architecture, as well as the pipelined NT/MP for one node and multiple NT/MP approaches, are very effective in reducing the latency.

We then evaluate the impact of varying the configurable parallelism factors supported by FlowGNN as a design space exploration (DSE). In particular, we observe how varying P_{node} , P_{edge} , P_{apply} , and P_{scatter} change the overall inference latency. The experiments use GCN model on MolHIV dataset. On top of the baseline architecture, we let $P_{\text{node}} \in \{1, 2, 4\}$, $P_{\text{edge}} \in \{1, 2, 4\}$, $P_{\text{apply}} \in \{1, 2, 4\}$, and $P_{\text{scatter}} \in \{1, 2, 4, 8\}$. 108 data points are plotted in Fig. 10, showing the speedup comparing to the baseline, where all four parameters are 1. First, each 3×3 block evaluates the impact of edge/node parallelism. In most cases, increasing P_{node} and P_{edge} lead to speedup, from $1.33 \times$ to $1.84 \times$ when both parameters increase from 1 to 4. We notice that in some cases, increasing one parameter does not change the latency. For example, in the left-most column, where $P_{\text{node}} = 1$, increasing P_{edge} does not lead to speedup. This indicates the scenarios where the message passing is not the bottleneck but the node transformation is. In such cases, increasing P_{node} can reduce latency. For instance, when $P_{\text{apply}} = 1$, $P_{\text{scatter}} = 2$, and $P_{\text{node}} = 1$, increasing P_{edge} from 2 to 4 does not change the speedup, but increasing P_{node} from 1 to 2 can improve the speedup to from $1.68 \times$ to $2.34 \times$. Second, increasing P_{apply} and P_{scatter} always seem effective (by looking at the values in the same position within the 3×3 blocks), from $1.09 \times$ to $2.99 \times$ when both parameters increase from 1 to 4. The largest speedup within the design space is $5.76 \times$, when $P_{\text{edge}} = 4$, $P_{\text{node}} = 2$, $P_{\text{apply}} = 4$, and $P_{\text{scatter}} = 8$. On the one hand, this DSE study demonstrates that increasing the four parallelism parameters can effectively reduce the model latency. On the other hand, we recognize that the speedup is not linear, e.g., doubling one parameter does not result in $2 \times$ speedup. One reason is the entangled effect of the four parameters, where some are the bottleneck while others are not; another reason is the imbalanced graphs resulting in imbalanced MP workload. We will consider the improvements in the future work.

5.5 Comparison Against GCN Accelerators

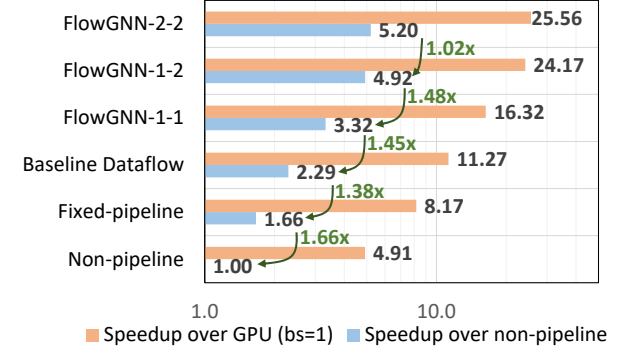


Figure 9: Effectiveness of the dataflow architecture in FlowGNN. Speedup plotted in log-scale. FlowGNN results are in the format of FlowGNN- P_{apply} - P_{scatter} .

Dataset	Accelerator	Latency (μs)	# of DSPs	Norm. by DSP
Cora	AWB-GCN	2.3	4096	2.3
	I-GCN	1.3	4096	1.3
	FlowGNN	6.912	747	1.261 (1.03×)
CiteSeer	AWB-GCN	4.0	4096	4.0
	I-GCN	1.9	4096	1.9
	FlowGNN	8.332	747	1.520 (1.25×)

Table 5: Comparison with I-GCN [15] and AWB-GCN [14] on the Cora and CiteSeer datasets using GCN. Although not a fair comparison, we still achieve $1.03 \times$ faster than I-GCN on Cora and $1.25 \times$ faster on CiteSeer.

As discussed earlier, most existing GNN accelerators focus on a form of GCN [27] that reduces to SpMM and is incapable of handling advanced features such as edge embeddings. I-GCN [15] and AWB-GCN [14] are two works of this type. In this section, we implement the GCN architecture of these existing works within the FlowGNN framework and compare its performance on the Cora and CiteSeer datasets. We follow their model configuration, using a two-layer GCN, with node embedding dimension being 16 and no edge embedding.

Results are shown in Table 5. Given the different hardware platform, we normalize by the number of DSPs, the major computation resource. Results show that after normalizing, we achieve $1.26 \times$ faster performance than I-GCN on Cora and $1.25 \times$ faster on CiteSeer, which is $1.8 \times$ and $2.6 \times$ faster than AWB-GCN, respectively. Although not a fair comparison because the optimizations in I-GCN and AWB-GCN do not generalize to edge embeddings, we still show superior performance.

6 CONCLUSION

In this work, we proposed **FlowGNN**, the first generic and flexible accelerator framework for a wide range of GNNs. It uses a novel dataflow architecture with multiple levels of parallelism, including edge/node and apply/scatter parallelism. The enabling techniques are multiple data queues with on-the-fly node multicasting. Its noteworthy features include generality for future-proofing, real-time processing, and open-source. On-board evaluation with guaranteed functionality exhibited invariant speed-up comparing with CPU and GPU baselines, up to $54\text{--}254 \times$ against CPU and $1.3\text{--}477 \times$ against

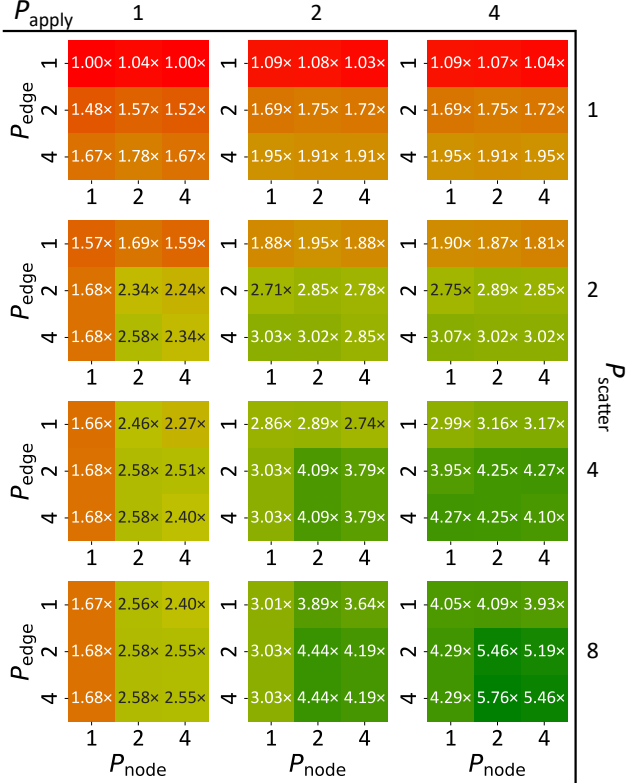


Figure 10: Overall speedup resulting from different parallelization factors P_{node} , P_{edge} , P_{apply} , and $P_{scatter}$.

GPU with batch sizes from 1024 to 1. We also outperform the SOTA GNN accelerator by $1.03\times$ and $1.25\times$. Remarkable speedup suggests that we did not sacrifice performance for generality and can deliver real-time performance.

ACKNOWLEDGEMENTS

The authors would like to thank Zihang Qiao for his contributions to the development of PNA and DGN, as well as Parima Mehta for her contribution to the virtual node model. The authors would also like to thank Dr. Pan Li for his insightful discussions.

REFERENCES

- [1] S. Abadal, A. Jain, R. Guirado, J. López-Alonso, and E. Alarcón, “Computing graph neural networks: A survey from algorithms to accelerators,” *ACM Computing Surveys*, vol. 54, no. 9, pp. 1–38, Dec. 2022.
- [2] K. Atz, F. Grisoni, and G. Schneider, “Geometric deep learning on molecular representations,” *Nature Machine Intelligence*, pp. 1–10, 2021.
- [3] A. Auten, M. Tomei, and R. Kumar, “Hardware acceleration of graph neural networks,” in *2020 57th ACM/IEEE Design Automation Conference (DAC)*. IEEE, 2020, pp. 1–6.
- [4] D. Beani, S. Passaro, V. Létourneau, W. Hamilton, G. Corso, and P. Lio, “Directional graph networks,” in *International Conference on Machine Learning*. PMLR, 2021, pp. 748–758.
- [5] G. Cerninara, A. Gupta, Y. Iiyama, J. Kieseler, V. Loncar, J. Ngadiuba, M. Pierini, M. Rieger, S. Summers, G. Van Onsem *et al.*, “Distance-weighted graph neural networks on FPGAs for real-time particle reconstruction at the Large Hadron Collider,” 2020.
- [6] X. Chen, Y. Wang, X. Xie, X. Hu, A. Basak, L. Liang, M. Yan, L. Deng, Y. Ding, Z. Du *et al.*, “Rubik: A hierarchical architecture for efficient graph neural network training,” *IEEE Transactions on Computer-Aided Design of Integrated Circuits and Systems*, 2021.
- [7] X. Chen, Y. Wang, X. Xie, X. Hu, A. Basak, L. Liang, M. Yan, L. Deng, Y. Ding, Z. Du, and Y. Xie, “Rubik: A hierarchical architecture for efficient graph neural network training,” *IEEE Transactions on Computer-Aided Design of Integrated Circuits and Systems*, vol. 41, no. 4, pp. 936–949, Apr. 2022.
- [8] X. Chen, H. Tan, Y. Chen, B. He, W.-F. Wong, and D. Chen, “Thundergp: Hls-based graph processing framework on fpgas,” in *The 2021 ACM/SIGDA International Symposium on Field-Programmable Gate Arrays*, 2021, pp. 69–80.
- [9] G. Corso *et al.*, “Principal neighbourhood aggregation for graph nets,” in *NeurIPS*, 2020.
- [10] G. Dai *et al.*, “GraphH: A processing-in-memory architecture for large-scale graph processing,” *IEEE TCAD*, vol. 38, no. 4, pp. 640–653, 2018.
- [11] G. Dai, T. Huang, Y. Chi, N. Xu, Y. Wang, and H. Yang, “Foregraph: Exploring large-scale graph processing on multi-fpga architecture,” in *Proceedings of the 2017 ACM/SIGDA International Symposium on Field-Programmable Gate Arrays*, 2017, pp. 217–226.
- [12] H. Gao and S. Ji, “Graph u-nets,” in *ICML*, 2019.
- [13] T. Geng, A. Li, R. Shi, C. Wu, T. Wang, Y. Li, P. Haghi, A. Tumeo, S. Che, S. Reinhardt *et al.*, “AWB-GCN: A graph convolutional network accelerator with runtime workload rebalancing,” in *2020 53rd Annual IEEE/ACM International Symposium on Microarchitecture (MICRO)*. IEEE, 2020, pp. 922–936.
- [14] T. Geng, A. Li, R. Shi, C. Wu, T. Wang, Y. Li, P. Haghi, A. Tumeo, S. Che, S. Reinhardt, and M. C. Herbordt, “AWB-GCN: A graph convolutional network accelerator with runtime workload rebalancing,” in *2020 53rd Annual IEEE/ACM International Symposium on Microarchitecture (MICRO)*. Athens, Greece: IEEE, Oct. 2020, pp. 922–936.
- [15] T. Geng, C. Wu, Y. Zhang, C. Tan, C. Xie, H. You, M. Herbordt, Y. Lin, and A. Li, “I-GCN: A graph convolutional network accelerator with runtime locality enhancement through islandization,” in *MICRO-54: 54th Annual IEEE/ACM International Symposium on Microarchitecture*. Virtual Event Greece: ACM, Oct. 2021, pp. 1051–1063.
- [16] J. Gilmer *et al.*, “Neural message passing for quantum chemistry,” in *ICML*, 2017.
- [17] L. Gong and Q. Cheng, “Exploiting edge features for graph neural networks,” in *Proceedings of the IEEE/CVF conference on computer vision and pattern recognition*, 2019, pp. 9211–9219.
- [18] W. L. Hamilton, R. Ying, and J. Leskovec, “Inductive representation learning on large graphs,” in *Proceedings of the 31st International Conference on Neural Information Processing Systems*, 2017, pp. 1025–1035.
- [19] W. Hu, M. Fey, M. Zitnik, Y. Dong, H. Ren, B. Liu, M. Catasta, and J. Leskovec, “Open graph benchmark: Datasets for machine learning on graphs,” in *Advances in Neural Information Processing Systems*, H. Larochelle, M. Ranzato, R. Hadsell, M. F. Balcan, and H. Lin, Eds., vol. 33. Curran Associates, Inc., 2020, pp. 22 118–22 133. [Online]. Available: <https://proceedings.neurips.cc/paper/2020/file/fb60d411a5c5b72b2e7d3527cfe84fd0-Paper.pdf>
- [20] W. Hu, B. Liu, J. Gomes, M. Zitnik, P. Liang, V. Pande, and J. Leskovec, “Strategies for pre-training graph neural networks,” 2019. [Online]. Available: <https://arxiv.org/abs/1905.12265>
- [21] Y. Iiyama, G. Cerninara, A. Gupta, J. Kieseler, V. Loncar, M. Pierini, S. R. Qasim, M. Rieger, S. Summers, G. Van Onsem *et al.*, “Distance-weighted graph neural networks on FPGAs for real-time particle reconstruction in high energy physics,” *Frontiers in big Data*, p. 44, 2021.
- [22] K. Ishiguro, S.-i. Maeda, and M. Koyama, “Graph warp module: an auxiliary module for boosting the power of graph neural networks,” *arXiv preprint arXiv:1902.01020*, 2019.
- [23] Z. Jia, S. Lin, R. Ying, J. You, J. Leskovec, and A. Aiken, “Redundancy-free computation for graph neural networks,” in *Proceedings of the 26th ACM SIGKDD International Conference on Knowledge Discovery & Data Mining*, 2020, pp. 997–1005.

[24] J. Kepner, H. Meyerhenke, S. McMillan, C. Yang, J. D. Owens, M. Zalewski, T. Mattson, J. Moreira, P. Aaltonen, D. Bader, A. Buluc, F. Franchetti, J. Gilbert, D. Hutchison, M. Kumar, and A. Lumsdaine, "Mathematical foundations of the GraphBLAS," in *2016 IEEE High Performance Extreme Computing Conference (HPEC)*. IEEE, sep 2016. [Online]. Available: <https://doi.org/10.1109%2Fhpec.2016.7761646>

[25] K. Kiningham, P. Levis, and C. Ré, "GReTA: Hardware optimized graph processing for GNNs," in *Proceedings of the Workshop on Resource-Constrained Machine Learning (ReCoML 2020)*, Mar. 2020.

[26] K. Kiningham, C. Re, and P. Levis, "GRIP: A graph neural network accelerator architecture," *arXiv:2007.13828 [cs]*, Jul. 2020.

[27] T. N. Kipf and M. Welling, "Semi-supervised classification with graph convolutional networks," in *ICLR*, 2016.

[28] J. Li, A. Louri, A. Karanth, and R. Bunescu, "GCNAX: A flexible and energy-efficient accelerator for graph convolutional neural networks," in *2021 IEEE International Symposium on High-Performance Computer Architecture (HPCA)*. Seoul, Korea (South): IEEE, Feb. 2021, pp. 775–788.

[29] L. Li, Y. Chen, Z. Zirnheld, P. Li, and C. Hao, "MELOPPR: Software/hardware co-design for memory-efficient low-latency personalized PageRank," in *2021 58th ACM/IEEE Design Automation Conference (DAC)*, 2021, pp. 601–606.

[30] S. Liang, Y. Wang, C. Liu, L. He, H. Li, D. Xu, and X. Li, "EnGN: A high-throughput and energy-efficient accelerator for large graph neural networks," *IEEE Transactions on Computers*, vol. 70, no. 9, pp. 1511–1525, 2021.

[31] S. Liang, Y. Wang, C. Liu, L. He, H. Li, D. Xu, and X. Li, "EnGN: A high-throughput and energy-efficient accelerator for large graph neural networks," *IEEE Transactions on Computers*, vol. 70, no. 9, pp. 1511–1525, Sep. 2021.

[32] "GNN models from Open Graph Benchmark," <https://github.com/snap-stanford/ogb/tree/master/examples/graphproppred/mol>, [Online; accessed 16-Jan-2022].

[33] T. Pham, T. Tran, H. Dam, and S. Venkatesh, "Graph classification via deep learning with virtual nodes," *arXiv preprint arXiv:1708.04357*, 2017.

[34] "PyTorch Geometric," <https://pytorch-geometric.readthedocs.io/en/latest/>, [Online; accessed 16-Jan-2022].

[35] P. Sen, G. Namata, M. Bilgic, L. Getoor, B. Galligher, and T. Eliassi-Rad, "Collective classification in network data," *AI magazine*, vol. 29, no. 3, pp. 93–93, 2008.

[36] Z. Shao, R. Li, D. Hu, X. Liao, and H. Jin, "Improving performance of graph processing on fpga-dram platform by two-level vertex caching," in *Proceedings of the 2019 ACM/SIGDA International Symposium on Field-Programmable Gate Arrays*, 2019, pp. 320–329.

[37] F. Shi, A. Y. Jin, and S.-C. Zhu, "Versagnn: a versatile accelerator for graph neural networks," *arXiv preprint arXiv:2105.01280*, 2021.

[38] W. Shi and R. Rajkumar, "Point-GNN: Graph neural network for 3D object detection in a point cloud," in *Proceedings of the IEEE/CVF conference on computer vision and pattern recognition*, 2020, pp. 1711–1719.

[39] J. Shlomi, P. Battaglia, and J.-R. Vlimant, "Graph neural networks in particle physics," *Machine Learning: Science and Technology*, vol. 2, no. 2, p. 021001, 2020.

[40] D. Szklarczyk, A. L. Gable, D. Lyon, A. Junge, S. Wyder, J. Huerta-Cepas, M. Simonovic, N. T. Doncheva, J. H. Morris, P. Bork *et al.*, "STRING v11: protein–protein association networks with increased coverage, supporting functional discovery in genome-wide experimental datasets," *Nucleic acids research*, vol. 47, no. D1, pp. D607–D613, 2019.

[41] S. A. Tailor, F. Opolka, P. Lio, and N. D. Lane, "Do we need anisotropic graph neural networks?" in *International Conference on Learning Representations*, 2021.

[42] Y. Tian *et al.*, "From" think like a vertex" to" think like a graph"," *VLDB*, vol. 7, no. 3, pp. 193–204, 2013.

[43] P. Veličković *et al.*, "Graph attention networks," in *arXiv preprint arXiv:1710.10903*, 2017.

[44] P. Veličković, "Message passing all the way up," 2022. [Online]. Available: <https://arxiv.org/abs/2202.11097>

[45] H. Wang *et al.*, "GCN-RL circuit designer: Transferable transistor sizing with graph neural networks and reinforcement learning," in *2020 57th ACM/IEEE Design Automation Conference (DAC)*. IEEE, 2020, pp. 1–6.

[46] Y. Wang, B. Feng, G. Li, S. Li, L. Deng, Y. Xie, and Y. Ding, "GNNAdviser: An efficient runtime system for GNN acceleration on GPUs," *arXiv preprint arXiv:2006.06608*, 2020.

[47] D. S. Wishart, Y. D. Feunang, A. C. Guo, E. J. Lo, A. Marcu, J. R. Grant, T. Sajed, D. Johnson, C. Li, Z. Sayeeda *et al.*, "DrugBank 5.0: a major update to the DrugBank database for 2018," *Nucleic acids research*, vol. 46, no. D1, pp. D1074–D1082, 2018.

[48] F. Wu *et al.*, "Simplifying graph convolutional networks," in *ICML*, 2019.

[49] Z. Wu, B. Ramsundar, E. N. Feinberg, J. Gomes, C. Geniesse, A. S. Pappu, K. Leswing, and V. Pande, "MoleculeNet: a benchmark for molecular machine learning," *Chemical science*, vol. 9, no. 2, pp. 513–530, 2018.

[50] K. Xu *et al.*, "How powerful are graph neural networks?" in *ICLR*, 2019.

[51] Y. Xue, Y. Liao, X. Chen, and J. Zhao, "Node augmentation methods for graph neural network based object classification," in *2021 2nd International Conference on Computing and Data Science (CDS)*. IEEE, 2021, pp. 556–561.

[52] D. Yan *et al.*, "Blogel: A block-centric framework for distributed computation on real-world graphs," *VLDB*, vol. 7, no. 14, pp. 1981–1992, 2014.

[53] M. Yan, L. Deng, X. Hu, L. Liang, Y. Feng, X. Ye, Z. Zhang, D. Fan, and Y. Xie, "HyGCN: A GCN accelerator with hybrid architecture," in *2020 IEEE International Symposium on High Performance Computer Architecture (HPCA)*. IEEE, 2020, pp. 15–29.

[54] M. Yan, L. Deng, X. Hu, L. Liang, Y. Feng, X. Ye, Z. Zhang, D. Fan, and Y. Xie, "HyGCN: A GCN accelerator with hybrid architecture," in *2020 IEEE International Symposium on High Performance Computer Architecture (HPCA)*. San Diego, CA, USA: IEEE, Feb. 2020, pp. 15–29.

[55] P. Yao, L. Zheng, X. Liao, H. Jin, and B. He, "An efficient graph accelerator with parallel data conflict management," in *Proceedings of the 27th International Conference on Parallel Architectures and Compilation Techniques*, 2018, pp. 1–12.

[56] Z. Yuan, Y. Yan, M. Sonka, and T. Yang, "Large-scale robust deep auc maximization: A new surrogate loss and empirical studies on medical image classification," in *Proceedings of the IEEE/CVF International Conference on Computer Vision*, 2021, pp. 3040–3049.

[57] H. Zeng and V. Prasanna, "GraphACT: Accelerating GCN training on CPU-FPGA heterogeneous platforms," in *Proceedings of the 2020 ACM/SIGDA International Symposium on Field-Programmable Gate Arrays*. Seaside CA USA: ACM, Feb. 2020, pp. 255–265.

[58] H. Zeng and V. Prasanna, "GraphACT: Accelerating GCN training on CPU-FPGA heterogeneous platforms," in *Proceedings of the 2020 ACM/SIGDA International Symposium on Field-Programmable Gate Arrays*, ser. FPGA '20. New York, NY, USA: Association for Computing Machinery, 2020, p. 255–265. [Online]. Available: <https://doi.org/10.1145/3373087.3375312>

[59] B. Zhang, R. Kannan, and V. Prasanna, "BoostGCN: A framework for optimizing GCN inference on FPGA," in *2021 IEEE 29th Annual International Symposium on Field-Programmable Custom Computing Machines (FCCM)*. IEEE, 2021, pp. 29–39.

[60] B. Zhang, H. Zeng, and V. Prasanna, "Hardware acceleration of large scale GCN inference," in *2020 IEEE 31st International Conference on Application-specific Systems, Architectures and Processors (ASAP)*. IEEE, 2020, pp. 61–68.

[61] S. Zhou, R. Kannan, V. K. Prasanna, G. Seetharaman, and Q. Wu, "Hitgraph: High-throughput graph processing framework on fpga," *IEEE Transactions on Parallel and Distributed Systems*, vol. 30, no. 10, pp. 2249–2264, 2019.